Many-fragment correlations and possible signature of spinodal fragmentation

B. Borderie, P. Désesquelles

EPJ manuscript No.
(will be inserted by the editor)

Many Fragment Correlations and Possible Signature of Spinodal Fragmentation

B. Borderie[1] and P. Désesquelles[2]

Institut de Physique Nucléaire, IN2P3-CNRS, F-91406 Orsay cedex, France
Centre de Spectrométrie Nucléaire et de Spectrométrie de Masse, IN2P3 et Université, F-91406 Orsay cedex, France

the date of receipt and acceptance should be inserted later

Abstract. Abnormal production of events with almost equal-sized fragments was theoretically proposed as a signature of spinodal instabilities responsible for nuclear multifragmentation. Many fragments correlations can be used to enlighten any extra production of events with specific fragment partitions. The high sensitivity of such correlation methods makes it particularly appropriate to look for small numbers of events as those expected to have kept a memory of spinodal decomposition properties and to reveal the dynamics of a first order phase transition for nuclear matter and nuclei. This section summarizes results obtained so far for both experimental and dynamical simulations data.

1 Introduction

Thermodynamics describes phase transitions in terms of static conditions. Information on the existence of phases and coexistence of phases is derived depending on thermodynamical parameters (temperature, pressure...). How to pass from a phase to another? What is the time needed? To answer these questions, dynamics of phase transitions must be studied. Therefore the aim of this section is to discuss signals which could be related to the dynamics of phase transition involved in hot unstable nuclei produced in nucleus-nucleus collisions . Of particular relevance is the possible occurrence of spinodal instabilities. Indeed, during a collision, a wide zone of the nuclear matter phase diagram may be explored and the nuclear system may enter the coexistence region (at low density) and even more precisely the unstable spinodal region (domain of negative compressibility). Thus, a possible origin of multifragmentation may be found through the growth of density fluctuations in this unstable region. Within this theoretical scenario a breakup into nearly equal-sized "primitive" fragments should be favoured. Hence many fragment correlations have been analyzed to investigate this possible scenario. They were applied on selected central collision events produced in experiments and also in 3D stochastic mean-field simulations of head-on collisions.

2 Spinodal instabilities for nuclear matter and nuclei

In the last fifteen years a big theoretical effort has been realized to understand and learn about spinodal decomposition in the nuclear context. A review can be found in reference [1].

2.1 Nuclear Matter

We shall first briefly discuss what are the specificities of spinodal decomposition as far as infinite nuclear matter is concerned. Associated to negative compressibility the mechanically unstable spinodal region can be investigated by studying the propagation of small density perturbations [2,3]. To do that the linear response framework is used to solve the RPA equations. In the spinodal region some modes do not oscillate but are amplified because of the instability. They have an imaginary eigenfrequency, this frequency being the inverse of the instability growth time. Figure 1 presents an example of nuclear dispersion

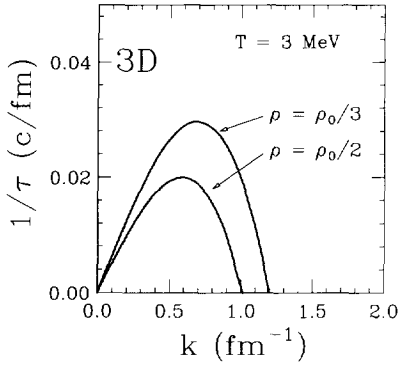

Fig. 1. Nuclear matter dispersion relation at 3 MeV temperature for two different densities; ρ_0 is the normal density. (from [2]).

relation at 3 MeV temperature for two different densities $\rho_0/2$ and $\rho_0/3$. Imaginary RPA frequencies are reported as a function of the wavenumber k of the considered perturbation. This dispersion relation exhibits a strong maximum at a given wave number followed by a cut-off at large k values. This cut-off reflects the fact that fluctuations with wavelength smaller than the range of the force can not be amplified. The most unstable modes correspond to wavelengths lying around $\lambda \approx 10$ fm and associated characteristic times are almost identical, around 30- 50 fm/c, depending on density ($\rho_0/2$-$\rho_0/8$) and temperature (0-9MeV) [2,4]. A direct consequence of the dispersion relation is the production of "primitive" fragments with size $\lambda/2 \approx 5$ fm which correspond to Z $\approx$ 10. However this simple and rather academic picture is expected to be largely blurred by several effects. We do not have a single unstable mode and consequently the beating of different modes occur. Coalescence effects due to the residual interaction between fragments before the complete disassembly are also expected [2].

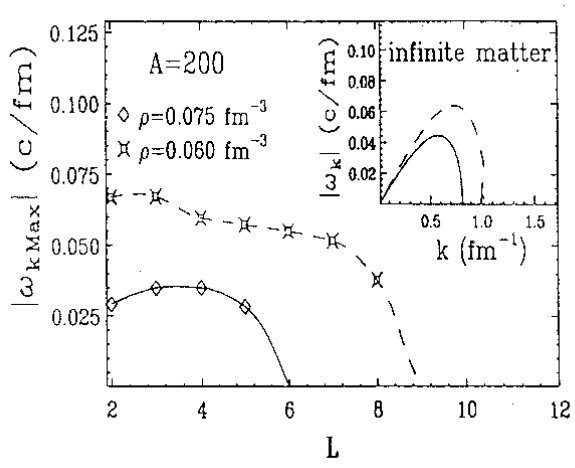

Fig. 2. Growth rates of the most unstable modes for a spherical source with 200 nucleons as a function of the multipolarity L and for two different central densities. (from [5]).

2.2 Finite systems

Does the signal discussed for nuclear matter survive (in final fragment partitions experimentally measured) if we consider the case of a hot expanding nucleus formed in heavy-ion collisions which undergoes multifragmentation?. First of all, the fused system produced has to stay long enough in the spinodal region (≈3 characteristic time: 100-150 fm/c) to allow an important amplification of the initial fluctuations. Second, the presence of a surface introduces an explicit breaking of the translational symmetry. Figure 2 shows the growth rates of the most unstable modes for a spherical source of A=200 with a Fermi shape profile and for two different central densities [5]. The growth rates are nearly the same for different multipolarities L up to a maximum multipolarity L_{max} (see also [6]). This result indicates that the unstable finite system breaks into different channels with nearly equal probabilities. Depending on multipolarity L, equal-sized "primitive" fragments are expected to be produced with sizes in the range $A_F/2$-A_F/L_{max}; A_F being the part of the system leading to fragments during the spinodal decomposition. One can also note that the Coulomb potential has a very small effect on the growth rates of unstable collective modes except close to the border of the spinodal zone where it stabilizes very long wave-length unstable modes [7].

On the other hand, for a finite system, Coulomb interaction reduces the freeze-out time and enhances the chance to keep a memory of the dynamical instabilities; a similar comment can be made if collective expansion of the system is present. Both effects push the "primitive" fragments one apart from the other and reduce the time of their mutual interaction.

3 Selected central collision events

Central collisions between medium or heavy nuclei leading to "fused" systems are very appropriate in the incident energy range 20-50 AMeV to produce well defined pieces of excited nuclear matter for which one could expect that bulk effects related to spinodal instabilities can occur. Such collisions represent a small (a few percent) part of cross-sections and corresponding events have been selected using global variables such as the total transverse energy E_t (^{129}Xe + ^{nat}Cu, ^{129}Xe + ^{197}Au and ^{36}Ar +^{197}Au at 50 AMeV)[9] or the flow angle (^{129}Xe + ^{nat}Sn for the incident energy domain 32-50 AMeV)[10] and the discriminant analysis method (^{58}Ni + ^{58}Ni and ^{58}Ni + ^{197}Au for the range 32-52 AMeV)[11,12,13].

4 Multi-fragment correlation functions and production of events with nearly equal-sized fragments

Following early studies related to nearly equal-sized fragment partitions [8], ten years ago a method called higher order charge correlations [9] was proposed to enlighten any extra production of events with specific fragment partitions. The high sensitivity of the method makes it particularly appropriate to look for small numbers of events as those expected to have kept a memory of spinodal decomposition properties. Thus, such a charge correlation method allows to examine model independent signatures that would indicate a preferred decay into a number of equal-sized fragments in events from experimental data or from simulations.

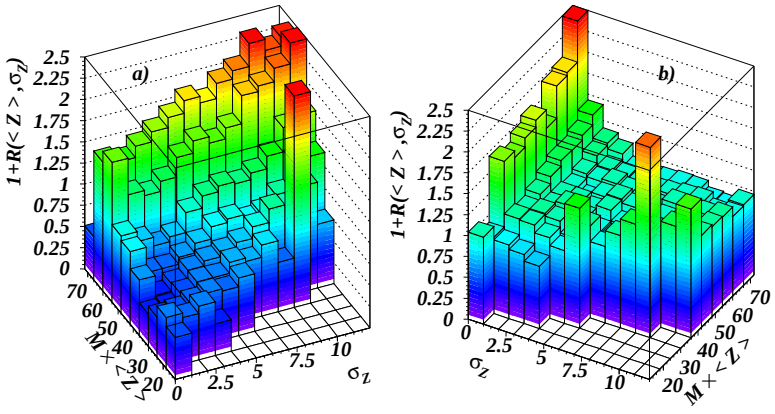

Fig. 3. Correlation functions for events with $M_f = 3$ to 6, simulated with the Brownian One Body model for 32 AMeV ^{129}Xe + ^{nat}Sn collisions. a) with an analytical denominator provided by FRM; b) with a denominator calculated with the IPM. The orientations of a) and b) are different for a better visualisation of the landscapes. (from[10]).

4.1 Methods

The classical two fragment charge correlation method considers the coincidence yield $Y(Z_1, Z_2)$ of two fragments of atomic numbers $Z_{1,2}$, in the events of multiplicity M_f of a sample. A background yield $Y'(Z_1, Z_2)$ is constructed by mixing, at random, fragments from different coincidence events selected by the same cut on M_f. The two particle correlation function is given by the ratio of these yields. When searching for enhanced production of events which break into equal-sized fragments, the higher order correlation method appears much more sensitive. All fragments of one event with fragment multiplicity $M_f = M = \sum_Z n_Z$, where n_Z is the number of fragments with charge Z in the partition, are taken into account. By means of the normalized first order:

$$\langle Z \rangle = \frac{1}{M} \sum_Z n_Z Z \tag{1}$$

and second order:

$$\sigma_Z^2 = \frac{1}{M} \sum_Z n_Z (Z - \langle Z \rangle)^2 \tag{2}$$

moments of the fragment charge distribution in the event, one may define the higher order charge correlation function as:

$$1 + R(\sigma_Z, \langle Z \rangle) = \left. \frac{Y(\sigma_Z, \langle Z \rangle)}{Y'(\sigma_Z, \langle Z \rangle)} \right|_M \tag{3}$$

Here, the numerator $Y(\sigma_Z, \langle Z \rangle)$ is the yield of events with given $\langle Z \rangle$ and σ_Z values. Because the measurement of the charge belonging to a given event is not subject to statistical fluctuations, one can use expression (2) rather than the "nonbiased estimator" of the variance, $\frac{1}{M-1} \sum_Z n_Z (Z - \langle Z \rangle)^2$, as proposed in [9] and also used in [14]. Note that this choice has no qualitative influence on the forthcoming conclusions. The denominator $Y'(\sigma_Z, \langle Z \rangle)$, which represents the uncorrelated yield of pseudo-events, was built in [9], as for classical correlation methods, by taking fragments at random in different events of the selected sample of a certain fragment multiplicity; this way to evaluate the denominator will be denoted as Fragments at Random Method (FRM) in what follows. This Monte-Carlo generation of the denominator $Y'(\sigma_Z, \langle Z \rangle)$ can be replaced by a fast algebraic calculation which is equivalent to the sampling of an infinite number of pseudo-events [15]. Its contribution to the statistical error of the correlation function is thus eliminated. However, owing to the way the denominator was constructed, only the fragment charge distribution $\mathrm{d}M/\mathrm{d}Z$ of the parent sample is reproduced but the constraints imposed by charge conservation are not taken into account. This has, in particular, a strong effect on the charge bound in fragments $\mathrm{d}M/\mathrm{d}Z_{\mathrm{bound}}$ distribution. This fact makes the denominator yield distributions as a function of $\langle Z \rangle$ wider and flatter than those of the numerator [16]. Consequently, even in the absence of a physical correlation signal, the ratio (3) is not a constant equal to one. The correlations induced by the finite size of the system (charge conservation) distorts the amplitude, or may even cancel other less trivial correlations. Therefore, a new method for the evaluation of the denominator [15], based on the "intrinsic probability" of emission of a given charge, was proposed. It minimizes these effects and replicates all features of the partitions of the numerator, except those (of interest) due to other reasons than charge conservation. The principle of the method is to take into account, in a combinatorial way, the trivial correlations due to charge conservation. If there is no correlation between the charges, each charge can be fully described by an emission probability referred to as intrinsic probability. This new method to build the denominator will be denoted as the Intrinsic Probability Method (IPM) in what follows. However, the explicit calculation of the intrinsic probabil-

ities may not be the only method for building a denominator including only the correlations induced by charge conservation. Another procedure was also proposed in [17]: the denominator is built by mixing events through random exchanges of two fragments between two events under the constraint that the sum of the two exchanged fragments is conserved, which satisfies $Z_{\rm bound}$ conservation (see also section 6 for a comparison with the IPM method). This last method will be denoted as the Random Exchange of Two Fragments Method (RETFM) in what follows.

4.2 Stochastic mean-field simulations and spinodal instabilities

Dynamical stochastic mean-field simulations have been proposed for a long time to describe processes involving instabilities like those leading to spinodal decomposition [18,19,20]. In this approach, spinodal decomposition of hot and dilute finite nuclear systems can be mimicked through the Brownian One-Body (BOB) dynamics [21, 22,23], which consists in employing a Brownian force in the kinetic equations. Simulations have been performed for head-on ^{129}Xe on ^{119}Sn collisions at 32 AMeV. The ingredients of simulations can be found in [23] as well as a detailed comparison between filtered simulated events (to account for the experimental device) and experimental data. A good agreement between both is revealed.

To refine the comparison higher-order charge correlations have been calculated for the simulated events [10], keeping the compact presentation proposed in [14]: charge correlation functions are built for all events, whatever their multiplicity, by summing the correlated yields for all M and by replacing the variable $\langle Z\rangle$ by $Z_{\rm bound} = M \times \langle Z\rangle = \sum_Z Z n_Z$. Uncorrelated events are constructed and weighted in proportion to real events of each multiplicity. This presentation is based on the experimental observation that the peaks observed independently for each fragment multiplicity correspond to the same $Z_{\rm bound}$ region [14]. The variance bin was chosen equal to one charge unit. One can recall that in the considered domain of excitation energy, around 3 MeV per nucleon [24,23], secondary evaporation leads to fragments one charge unit smaller, on average, than the primary $Z \approx 10-20$ ones, with a standard deviation around one [16]. If a weak enhanced production of exactly equal-sized fragments exists, peaks are expected to appear in the interval $\sigma_Z = 0-1$, because of secondary evaporation. This interval in σ_Z is hence the *minimum* value which must be chosen to look for nearly equal-sized fragments. Any (unknown) intrinsic spread in the fragment size coming from the break-up process itself may enlarge the σ_Z interval of interest. Here, only events with $\sigma_Z < 1$ were considered, which corresponds to differences of at most two units between the fragment atomic numbers in one event.

Fig. 3 shows the correlation function calculated using the analytical denominator of FRM (a) or the denominator given by the IPM (b). Both functions are drawn versus the variables $Z_{\rm bound} = M \times \langle Z\rangle$ and σ_Z. In fig. 3a, the

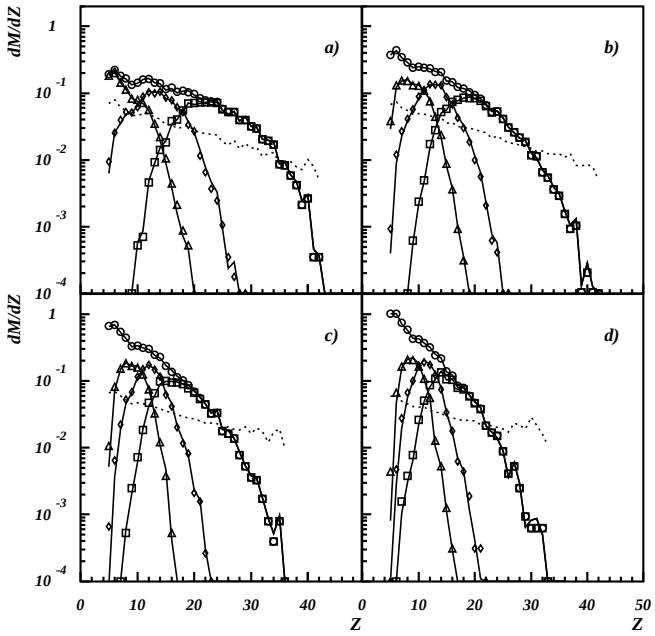

Fig. 4. Experimental differential charge multiplicity distributions (circles) for the single source formed in central 39 AMeV ^{129}Xe on ^{nat}Sn collisions. Parts a, b, c and d refer respectively to fragment multiplicities 3, 4, 5, 6. The Z distributions for the first (squares), second (diamonds) and third (triangles) heaviest fragments are presented too. The lines correspond to the results obtained with IPM. The dashed lines display the intrinsic probabilities. (from[10]).

equal-sized fragment correlations in the first bin are superimposed over trivial correlations due to the finite size of the system. For this reason, the ratio (3) is generally different from one and smoothly varies with the variables $Z_{\rm bound}$ and σ_Z. For each bin in $Z_{\rm bound}$ (fixed at 6 atomic number units), an exponential evolution of the correlation function is observed from $\sigma_Z = 7-8$ down to $\sigma_Z = 2-3$. This exponential evolution was thus taken as a "background" empirically extrapolated down to the first bin $\sigma_Z = 0-1$. The amplitude of the correlation function in the domain $Z_{\rm bound} = 36-60$ is well above the background, with a confidence level higher than 90%, proving thus a statistically significant enhancement of equal-sized fragment partitions. Of the 1% of events having $\sigma_Z < 1$, (0.13±0.02)% (called extra-events from now on) are in excess of the background. In fig. 3b, as one could expect, all correlations due to the charge conservation are suppressed and the correlation function is equal to 1 (within statistical fluctuations) wherever no additional correlation is present. Again peaks for $\sigma_Z < 1$ are observed. The percentage of extra-events is 0.36±0.03%, higher than the one obtained with the previous method. Moreover, with this method, peaks also appear at the maximum values of σ_Z for a given $Z_{\rm bound}$. They correspond to events composed of one big (a heavy residue) and several lighter fragments (sequentially emitted from the big one). In that case fusion-multifragmention does not occur and the peaks re-

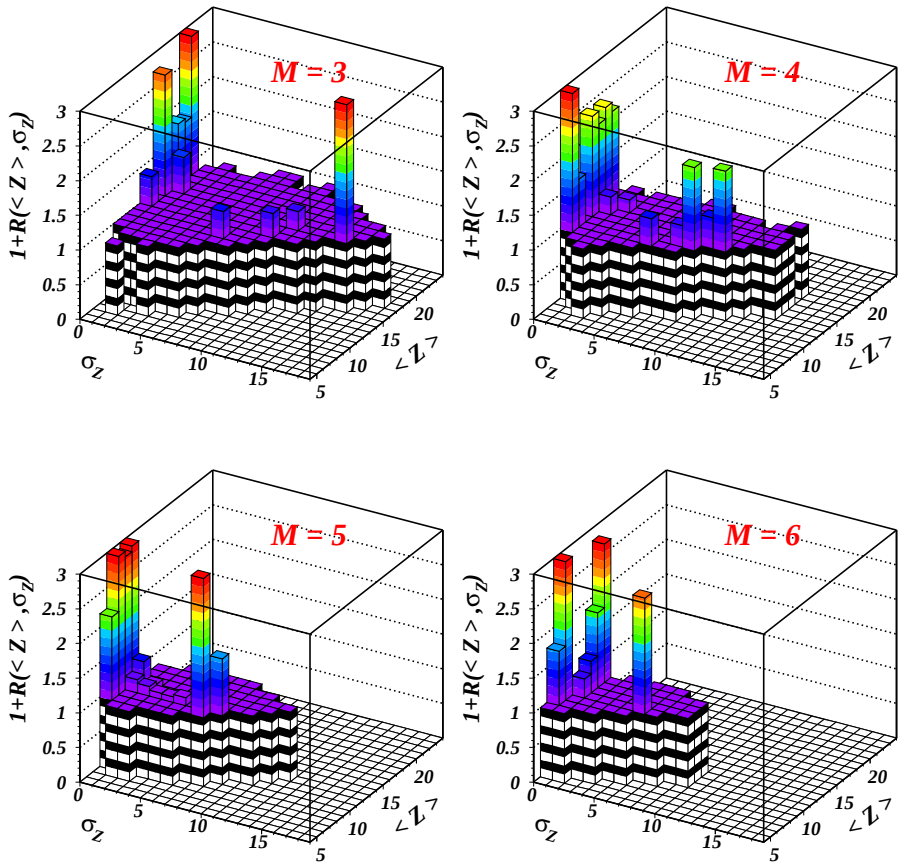

Fig. 5. Experimental higher-order charge correlations for selected events formed in central 39 AMeV ^{129}Xe on ^{nat}Sn collisions, for fragment multiplicities 3 to 6. The maximum value of the scale of the correlation function is limited to 3 on the picture. (from[10]).

veal the small proportion (0.15%) of events which undergo the fusion-evaporation process.

Note that very recently higher order charge correlations were also studied for central Ni+Ni collisions simulated using LATINO semiclassical model [25]. A single source at 4.75 AMeV excitation energy was measured, which deexcites with an abnormal production of four equal sized fragments.

To conclude this part one can say that, although all events in the simulation arise from spinodal decomposition, only a very small fraction of the final partitions have nearly equal-sized fragments. Let recall again that different effects: beating of different modes, coalescence of nascent fragments, secondary decay of the excited fragments and, above all, finite size effects are responsible for this fact [5,2]. The signature of spinodal decomposition can only reveal itself as a "fossil" signal.

4.3 Experimental results

As an example, higher-order charge correlations for selected experimental events concerning ^{129}Xe on ^{nat}Sn collisions at 39 AMeV incident energy [10] are presented. This is in the framework of the IPM for the denominator. The first step consists in determining the intrinsic probabilities of fragments for each multiplicity. These probabilities are obtained by a recursive procedure of minimization. The minimization criterion is the normalized χ^2 between experimental and combinatorial fragment partition probabilities. Charge distributions experimentally observed for the different fragment multiplicities are shown in fig. 4. Dashed lines refer to the intrinsic probabilities calculated with IPM and the corresponding charge distributions are the full lines. One can note the excellent agreement between calculations and data. The contributions to the Z distribution of the three heaviest fragments of each partition are also well described and the charges bound in fragments (not shown) are perfectly reproduced.

Fig. 5 illustrates the higher-order correlation functions measured for the different fragment multiplicities. To make the effects more visible, peaks with confidence level lower than 80% were flattened out. We observe significant peaks in the bin $\sigma = 0 - 1$ for each fragment multiplicity. For M=6, peaks are essentially located in the bin $\sigma_Z = 1 - 2$. As observed in simulations, peaks corresponding to events composed of a heavy residue and light fragments (σ_Z in the region 5-10 associated with low $\langle Z \rangle$) are also visible.

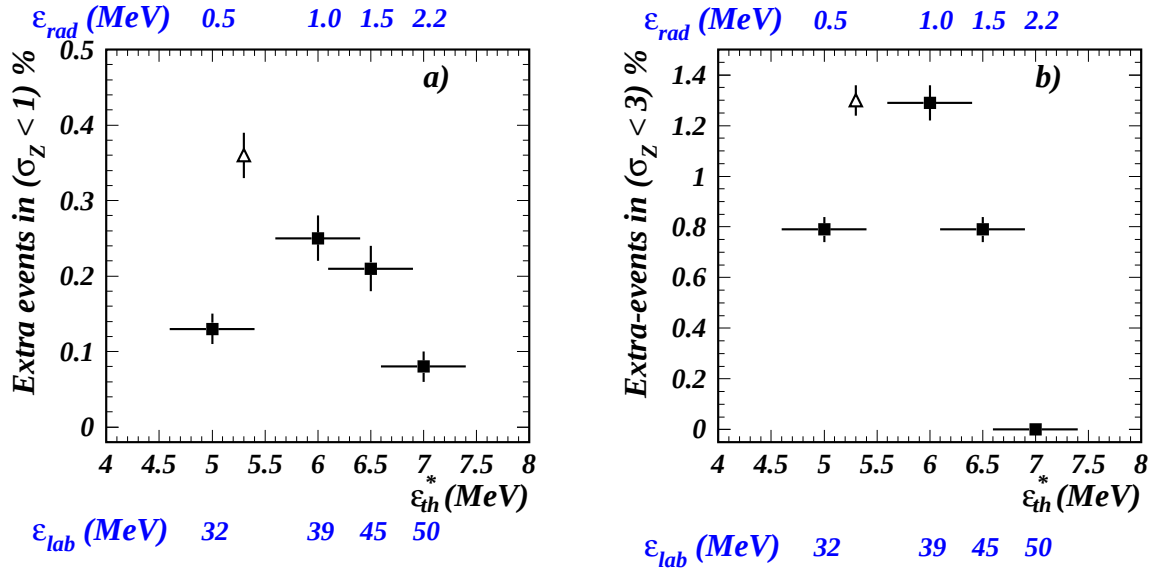

Fig. 6. Abnormal production of events with nearly equal-sized fragments (a: $\sigma_Z < 1$ and b: $\sigma_Z < 3$) as a function of thermal excitation energy (full points); the incident and radial energy scales are also indicated. ϵ^*_{th} and ϵ_{rad} are deduced from comparisons with SMM. The open point refers to the result from BOB simulations; the average thermal excitation energy is used. Vertical bars correspond to statistical errors and horizontal bars refer to estimated uncertainties on the backtraced quantity, ϵ^*_{th}. (from[10]).

Table 1. World-wide results on fragment correlations. DA refers to the Discriminant Analysis method. Percentage of extra events refers to the extra-percentage of events with nearly equal-sized fragments which correspond to $\sigma_Z < 1$.

system	energy (AMeV)	source selection	detection (% of Zsyst)	correlation method	$< Z >$ range	percentage of extra events	ref
^{129}Xe + ^{nat}Cu	50	top 5% E_t	-	FRM	-	no events	[9]
^{129}Xe + ^{197}Au	50	top 5% E_t	-	FRM	-	no events	[9]
^{36}Ar + ^{197}Au	50	top 5% E_t	-	FRM	-	no events	[9]
^{129}Xe + ^{119}Sn	32	BOB (b=0)	INDRA filter	FRM	10-19	0.13	[10]
^{129}Xe + ^{119}Sn	32	BOB (b=0)	INDRA filter	IPM	8-20	0.36	[10]
^{129}Xe + ^{119}Sn	32	BOB (b=0)	INDRA filter	RETFM	-	no events	[27,28]
^{129}Xe + ^{nat}Sn	32	$\theta_{flow} > 60°$	>80%	FRM	10-19	0.10	[14]
"	32	$\theta_{flow} > 60°$	>80%	IPM	11-21	0.13	[10]
"	32	$\theta_{flow} > 60°$	>80%	RETFM	-	no events	[17]
^{129}Xe + ^{nat}Sn	39	$\theta_{flow} > 60°$	>80%	IPM	6-20	0.25	[10]
"	39	$\theta_{flow} > 60°$	>80%	RETFM	-	no events	[17]
^{129}Xe + ^{nat}Sn	45	$\theta_{flow} > 60°$	>80%	IPM	6-18	0.21	[10]
"	45	$\theta_{flow} > 60°$	>80%	RETFM	-	no events	[17]
^{129}Xe + ^{nat}Sn	50	$\theta_{flow} > 60°$	>80%	IPM	7-9	0.08	[10]
"	50	$\theta_{flow} > 60°$	>80%	RETFM	-	no events	[17]
^{58}Ni + ^{197}Au	32	DA (SIMON training)	>60%	IPM	-	no events	[12]
^{58}Ni + ^{197}Au	52	DA (SIMON training)	>60%	IPM	7-15	not given	[12]
^{58}Ni + ^{58}Ni	32	DA (data training)	>80%	IPM	-	no events	[13]
^{58}Ni + ^{58}Ni	40	DA (data training)	>80%	IPM	5	events ?	[13]
^{58}Ni + ^{58}Ni	52	DA (data training)	>80%	IPM	4-8	0.85	[13]

At 32 AMeV incident energy, for the same system, similar results were obtained using FRM or IPM methods and well compare to those obtained with events from dynamical simulations, BOB [14,10]. On the other hand no abnormal production of events with nearly equal-sized fragments was obtained using the RETFM [17].

Moreover, using the IPM method, a rise and fall of the percentage of "fossil partitions" from spinodal decomposition is measured over the incident energy range 32-50 AMeV (see Fig. 6) The percentages of events with $\sigma_Z < 3$ are also reported. The conclusions are the same: while more events have small values of σ_Z when the incident energy increases, the percentage of extra-events shows a maximum at 39 AMeV but vanishes at 50 AMeV. Fig. 6 also reveals some difference between the experimental (full symbols) and simulated events (open symbols): the exper-

imental percentages of extra events are closer to the simulated ones in fig. 6b than in fig. 6a. This means that the charge distributions inside an event are slightly narrower in the simulation than in the experiment either because of the primary intrinsic spread, or because the width due to evaporation is underestimated. For the considered system, incident energies around 35-40 AMeV could appear as the most favourable to induce spinodal decomposition; it corresponds to about 5.5-6 AMeV thermal excitation energy associated to a very gentle expansion energy around 0.5-1 AMeV. The qualitative explanation for those numbers can be well understood in terms of a necessary compromise between two times. On one hand the fused systems have to stay in the spinodal region $\approx$ 100-150 fm/c [2, 4, 26], to allow an important amplification of the initial fluctuations and thus permit spinodal decomposition; this requires a not too high incident energy, high enough however for multifragmentation to occur. On the other hand, for a finite system, Coulomb interaction and collective expansion push the "primitive" fragments apart and reduce the time of their mutual interaction, which is efficient to keep a memory of "primitive" size properties. Note that such an explanation can not be derived using the RETFM for which no abnormal production of events with nearly equal-sized fragments was measured, neither in BOB simulations [27, 28] nor in experimental data [17].

Table 1 summarizes all the results concerning charge correlation studies performed up to now.

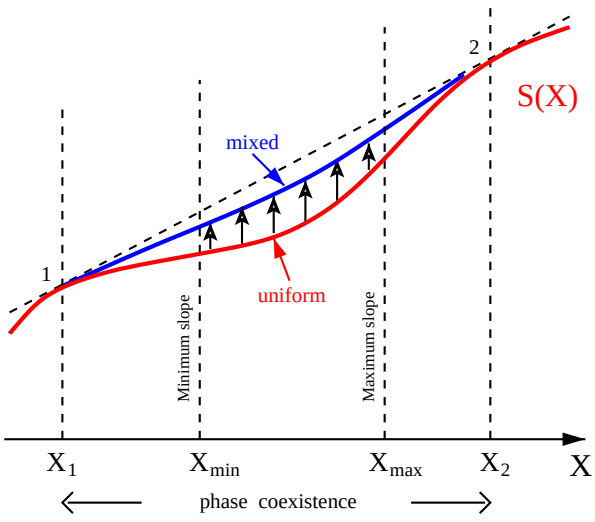

Fig. 7. Isolated finite system. The entropy function for a uniform system (lower curve) has a convexity region and the system gains entropy reorganizing itself into two subsystems but the resulting equilibrium entropy function (upper curve) will always lie below the common tangent (dashed line); from [1].

5 Observation of correlated signals

The concept of spinodal instability applies in general to macroscopically uniform systems that are suddenly brought into the coexistence region of their phase diagram. This instability occurs when the entropy function for the uniform system has a local convexity. Then the system splits into two independent subsystems (spinodal decomposition) to increase entropy; in the thermodynamical limit the entropy is additive and the Maxwell construction operates. For finite systems these features are no more correct. Interfaces between coexisting phases are no longer negligible and the entropy at equilibrium does not correspond to the sum of the individual subsystem entropies: the Maxwell construction is no more valid as illustrated in figure 7. Thus one can stress an important fact related to finite systems. It concerns the sign of the heat capacity in the spinodal region: if spinodal decomposition is observed, one must measure correlatively a negative microcanonical heat capacity related to the resulting equilibrium entropy function with local convexity.

Both signals (spinodal decomposition and negative microcanonical heat capacity) have been simultaneously studied on different fused systems which undergo multifragmentation [29, 10, 12, 13]. Results are summarized in table 2. For the different systems we have also indicated the associated thermal and radial collective energies derived from data. We generally observe a correlation between the two signals. They are present when a total (thermal+radial) energy in the range 5.5-8.0 AMeV is measured. Note that the effect of a very gentle compression phase leading to 0.5-1.0 AMeV radial expansion energy seems to play the same role as a slightly higher thermal energy (Ni+Au system at 52 AMeV). This can be understood in terms of a required threshold for expansion energy; in the latter case this threshold should be reached by thermal expansion only.

6 Correlation methods and confidence level

As we have seen in section 4, very different results are obtained for the ^{129}Xe + ^{nat}Sn system using IPM or RETFM for the calculation of the denominator. The sensitivity of the two methods was tested [10] by building correlation functions $1 + R(\sigma_Z, \langle Z \rangle)$ with σ_Z being calculated from eq. 2. The results of the two methods are compared in fig. 8 and fig. 9, displaying for each bin of the plane (σ_Z, M $\times \langle Z \rangle$), the deviation from 1, $R(\sigma_Z, \langle Z \rangle)$, of the correlation function, normalized to its statistical error bar, $\sigma_{1+R(\sigma_Z,\langle Z \rangle)}$, calculated from the numerator only.

The greater sensitivity of the IPM appears in fig. 8: the values of the correlation function are closer to one (R=0) except at low σ_Z where one observes correlations with significant confidence level (2 to 4 σ_{1+R}). Conversely, the exchange method, fig. 9, leads to a large dispersion of the values of $R(\sigma_Z, \langle Z \rangle)/\sigma_{1+R(\sigma_Z,\langle Z \rangle)}$, $\sim$1.6 times broader than with the IPM at 32, 39 and 45 AMeV. This observation may be related to the fact that in the IPM one adjusts the partition probabilities. Thus all experimental charge

Table 2. Summary of the findings for phase transition signals.

system	Ni+Au	Ni+Ni	Xe+Sn	Xe+Sn	Ni+Au	Ni+Ni	Xe+Sn	Xe+Sn	Ni+Ni
Incident Energy AMeV	32.	32.	32.	39.	52.	40.	45.	50.	52.
Thermal energy AMeV	5.0±1.0	5.0±1.0	5.0±0.5	6.0±0.5	6.0±1.0	6.3±1.0	6.5±0.5	7.0±0.5	8.0±1.0
Radial energy AMeV	0.	0.8±0.5	0.5±0.2	1.0±0.3	0.	1.7±0.5	1.5±0.4	2.2±0.4	2.4±0.5
Spinodal decomposition	no	no	yes	yes	yes	yes?	yes	no	yes
Negative microc. heat capacity	no	yes	yes	yes	yes	yes?	yes?	no	no

distributions are reproduced (see fig. 4) whereas in the RETFM only the distribution of the total charge emitted in fragments, Z_{bound}, is constrained. So the IPM approach should appear more suitable to reveal weak correlations.

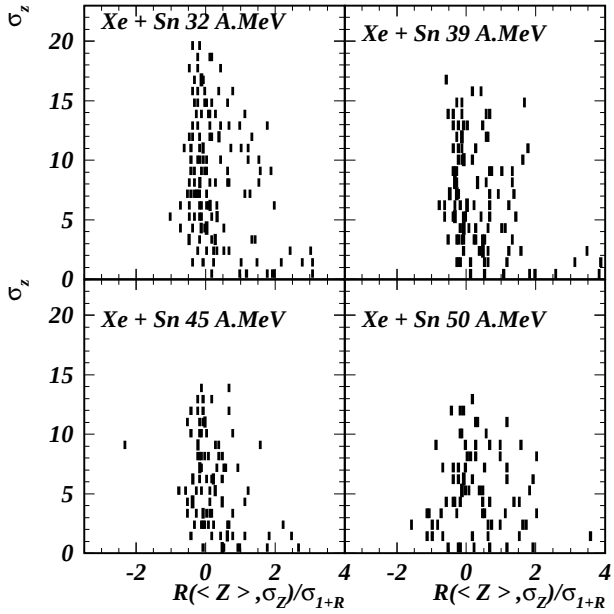

Fig. 8. Deviations from 1 of the correlation functions divided by the statistical errors in abcissa, for the different values of σ_Z. Correlation functions calculated by the IPM. (from[10]).

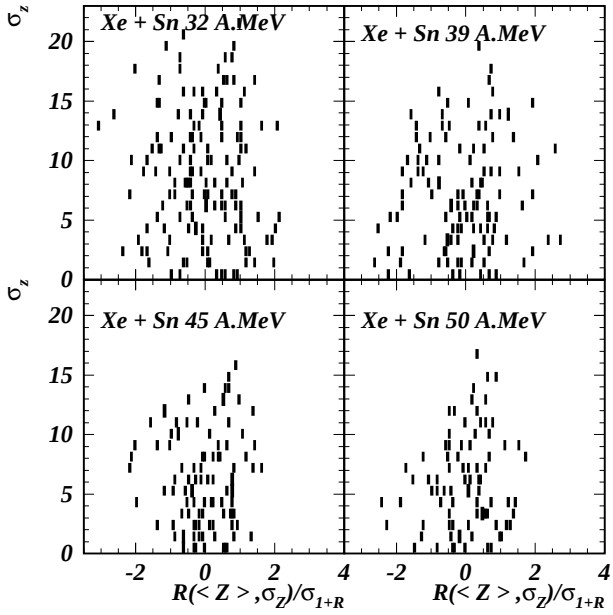

Fig. 9. Deviations from 1 of the correlation functions divided by the statistical errors in abcissa, for the different values of σ_Z. Correlation functions calculated by the RETFM. (from[10]).

7 Perspectives

Charge correlation functions for compact fused systems which undergo multifragmentation have been investigated, as a function of the incident energy, from 30 to 50 AMeV. Enhanced production of events with almost equal-sized fragments at the level of 0.1-0.8% were possibly revealed. Supported by theoretical simulations this abnormal enhancement can be interpreted as a signature of spinodal instabilities as the origin of multifragmentation in the Fermi energy domain. This fossil signal seems to culminate for incident energy around 35-40 AMeV. Microcanonical heat capacities observed in correlation with fossil signals also plead for spinodal decomposition to describe the dynamics of a phase transition for hot nuclei. However confidence levels, lower than 5 σ_{1+R}, observed for charge correlations prevent any definitive conclusion.

To firmly assess or not the validity of this fossil signal new studies must be performed:

- by achieving new experiments with higher statistics to reach relevant confidence levels,

- by performing dynamical simulations at higher incident energies and for different impact parameters,

- by increasing, on same event samples, the cross-check of different signals predicted to be correlated.

Moreover more direct experimental determinations of thermal and radial energies of fragment sources are required to better determine the domain where "fossil partitions" are produced and preserved.

References

1. P. Chomaz, M. Colonna and J. Randrup, Phys. Rep. **389**, 263 (2004).
2. M. Colonna, P. Chomaz and A. Guarnera, Nucl. Phys. **A 613**, 165 (1997).
3. S. Ayik, M. Colonna and P. Chomaz, Phys. Lett. **B 353**, 417 (1995).
4. D. Idier, M. Farine, B. Remaud and F. Sébille, Ann. Phys. Fr. **19**, 159 (1994).
5. B. Jacquot, S. Ayik, P. Chomaz and M. Colonna, Phys. Lett. **B 383**, 247 (1996).
6. W. Nörenberg, G. Papp and P. Rozmej, Eur. Phys. J. **A 9**, 327 (2000).
7. B. Jacquot, thèse de doctorat, Université de Caen (1996), GANIL T 96 05.
8. M. Bruno *et al.*, Phys. Lett. **B 292**, 251 (1992); Nucl. Phys. **A 576**, 138 (1994);
9. L. G. Moretto, T. Rubehn, L. Phair, N. Colonna, G. J. Wozniak *et al.*, Phys. Rev. Lett. **77**, 2634 (1996).
10. G. Tăbăcaru, B. Borderie, P. Désesquelles, M. Pârlog, M. F. Rivet *et al.*, Eur. Phys. J. **A 18**, 103 (2003).
11. P. Désesquelles, A. M. Maskay, P. Lautesse, A. Demeyer, E. Gerlic *et al.* (INDRA Collaboration), Phys. Rev. **C 62**, 024614 (2000).
12. B. Guiot, thèse de doctorat, Université de Caen (2002), http://tel.ccsd.cnrs.fr/documents/archives0/00/00/37/53/.
13. R. Moustabchir, thèse de doctorat, Université Claude Bernard - Lyon I et Université Laval Québec (2004), http://tel.ccsd.cnrs.fr/documents/archives0/00/00/86/54/.
14. B. Borderie, G. Tăbăcaru, P. Chomaz, M. Colonna, A. Guarnera *et al.* (INDRA Collaboration), Phys. Rev. Lett. **86**, 3252 (2001).
15. P. Désesquelles, Phys. Rev. C **65**, 034604 (2002).
16. G. Tăbăcaru, thèse de doctorat, Université Paris-XI Orsay (2000), http://tel.ccsd.cnrs.fr/documents/archives0/00/00/79/12/.
17. J. L. Charvet, R. Dayras, D. Durand, O. Lopez, D. Cussol *et al.*, Nucl. Phys. **A 730**, 431 (2004).
18. J. Randrup and B. Remaud, Nucl. Phys. **A 514**, 339 (1990).
19. P. Chomaz, G. F. Burgio and J. Randrup, Phys. Lett. **B 254**, 340 (1991).
20. G. F. Burgio, P. Chomaz and J. Randrup, Nucl. Phys. **A 529**, 157 (1991).
21. P. Chomaz, M. Colonna, A. Guarnera and J. Randrup, Phys. Rev. Lett. **73**, 3512 (1994).
22. A. Guarnera, P. Chomaz, M. Colonna and J. Randrup, Phys. Lett. **B 403**, 191 (1997).
23. J. D. Frankland, B. Borderie, M. Colonna, M. F. Rivet, C. O. Bacri *et al.* (INDRA Collaboration), Nucl. Phys. **A 689**, 940 (2001).
24. N. Marie, A. Chbihi, J. Natowitz, A. Le Fèvre, S. Salou *et al.* (INDRA Collaboration), Phys. Rev. **C 58**, 256 (1998).
25. A. Barranon and J. A. Lopez, nucl-th/0503070 (2005).
26. W. Nörenberg, G. Papp and P. Rozmej, Eur. Phys. J. **A 14**, 43 (2002).
27. M. F. Rivet *et al.* (INDRA collaboration), G. Agnello, A. Pagano and S. Pirrone, eds., *Proc. Int. Workshop on Multifragmentation 2003, GANIL, Caen, France* (2003), 22, `nucl-ex/0501008`.
28. M. F. Rivet, N. Le Neindre, J. Wieleczko, B. Borderie, R. Bougault *et al.* (INDRA and ALADIN collaborations), Nucl. Phys. **A 749**, 73 (2005).
29. N. Le Neindre, thèse de doctorat, Université de Caen (1999), http://tel.ccsd.cnrs.fr/documents/archives0/00/00/37/41/.